catalysts

MDPI

Article

The Effect of Citric Acid Concentration on the Properties of $LaMnO_3$ as a Catalyst for Hydrocarbon Oxidation

Zakaria Sihaib [1,2], Fabrizio Puleo [2], Giuseppe Pantaleo [2], Valeria La Parola [2], José Luis Valverde [3], Sonia Gil [1,*], Leonarda Francesca Liotta [2,*] and Anne Giroir-Fendler [1,*]

1 Université de Lyon, Université Lyon 1, CNRS, UMR 5256, IRCELYON, 69626 Villeurbanne CEDEX, France; zakaria.sihaib@ircelyon.univ-lyon1.fr

2 Istituto per lo Studio dei Materiali Nanostrutturati (ISMN)-CNR, 90146 Palermo, Italy; fabrizio.puleo@ismn.cnr.it (F.P.); giuseppe.pantaleo@ismn.cnr.it (G.P.); valeria.laparola@ismn.cnr.it (V.L.P.)

3 Facultad de Ciencias y Tecnologías Quimicas, Departamento de Ingenieria Quimica, Universidad de Castilla-La Mancha, 13071 Ciudad Real, Spain; JoseLuis.Valverde@uclm.es

* Correspondence: sonia.gil@ircelyon.univ-lyon1.fr (S.G.); leonarda.liotta@ismn.cnr.it (L.F.L.); anne.giroir-fendler@ircelyon.univ-lyon1.fr (A.G.-F.); Tel.: +33-472-431-054 (S.G.); +39-091-6809371 (L.F.L.); +33-472-431-586 (A.G.-F.); Fax: +39-091-6809399 (L.F.L.); +33-472-431-695 (A.G.-F.)

Received: 21 December 2018; Accepted: 23 February 2019; Published: 1 March 2019

Abstract: $LaMnO_3$ (LM) catalysts with a molar ratio of citric acid (CA) to metal (La^{3+} + Mn^{2+}) nitrates ranging from 0.5 to 2 (LM0.5 to LM2) were synthesized by the citrate sol–gel method with the aim of studying the effect of the citric acid ratio on the physicochemical properties and the catalytic performance in hydrocarbon oxidation. Structural and morphological properties of these catalysts were characterized by X-ray diffraction (XRD) and specific surface area (N_2 adsorption) measurements, while the chemical composition was determined by inductively coupled plasma atomic emission spectroscopy (ICP-OES). In the selected samples, additional characterizations were carried out by thermogravimetric and differential thermal analysis (TGA/DTA), Fourier Transform Infrared Spectroscopy (FT-IR), temperature-programmed reduction by hydrogen (H_2-TPR), and X-ray photoelectron spectroscopy (XPS). The results showed that the amount of citric acid used significantly influenced the TGA/DTA profile of gels along with the physicochemical properties of the catalysts. The XRD patterns are consistent with the perovskite formation as the main phase. The segregation of a small amount of Mn_3O_4, detected for molar ratios ranging between 0.5 and 1.5, suggested the formation of a slightly nonstoichiometric $LaMn_{1-x}O_3$ phase with a relatively high content of Mn^{4+}. The catalytic performance was evaluated in the total oxidation of two selected hydrocarbons, toluene and propene, which represent typical volatile organic compounds (VOCs). Typically, three consecutive catalytic cycles were performed in order to reach steady-state performance in toluene and propene oxidation. Moreover, the stability of the catalysts under reaction conditions was investigated through 24-h experiments at 17% of toluene conversion. The catalysts LM1.2, LM1.3, and LM1.5 showed the best catalytic performance in both hydrocarbon oxidations, well comparing with the Pd/Al_2O_3 used as a reference.

Keywords: $LaMnO_3$ perovskite; citric acid/metal nitrates molar ratio; structural and morphological characterization; toluene and propene total oxidation

1. Introduction

Catalysts based on lanthanum manganites ($LaMnO_3$) with a perovskite structure have attracted wide interest in the last few decades due to their potential application in electrocatalysis and solid

oxide fuel cells [1–3], as semiconductors thanks to their giant magnetoresistance properties [4], and in catalysis, especially for NO_x removal [5–7] and methane, CO, and VOCs oxidation [8–16]. Since the early investigations elucidating the peculiar activity of $LaMnO_3$-based perovskites in CO oxidation and the important role played by oxygen mobility [17], many further studies have been carried out to elucidate the relationships between the solid-state properties and their catalytic activity. It has been demonstrated that the introduction of surface defects as well as the modification of surface features directly affect the properties [18]. The catalytic combustion of acetone, isopropanol, and benzene have been investigated over $LaMnO_3$ perovskites, revealing that the presence of surface oxygen species, easily available and sufficiently mobile, was fundamental to the high catalytic activity of $LaMnO_3$ [19]. A strong correlation between oxygen mobility and the rate of N_2O decomposition was found in $La_{1-x}Sr_xMnO_3$ samples prepared by the Pechini route [20]. The highest values of the content of fast-exchangeable oxygen and oxygen diffusion coefficient were found for a multiphase sample containing layered perovskite, providing a strong correlation between oxygen mobility and catalytic activity.

According to these findings, the principal goal, leading to great enhancement of catalytic properties, is the improvement of the textural properties of $LaMnO_3$ perovskites, increasing the exposed specific surface, enhancing the surface and bulk oxygen mobility, and increasing the average oxidation state of Mn (a higher proportion of Mn^{4+} with respect to Mn^{3+}). Many efforts have been made to this end, resulting in the development of more efficient synthesis routes, such as co-precipitation [21,22], complexation [17,23], freeze/spray drying [22,24–26], and sol–gel [27], as well as explosion processes [28,29] and high-energy ball milling [30,31]. Recently, sol–gel synthesis has emerged as an attractive technique for the production of high-purity and crystalline oxide powders at a significantly lower temperature than the conventional synthesis method [32,33].

In a previous work [34], some of us successfully prepared $LaMnO_3$ perovskite by sol-gel for the oxidation of toluene, using a CA to total metal ions (La^{3+} + Mn^{2+}) molar ratio fixed at 1.5, whose catalytic performance was compared to that of other manganese oxide-based catalysts. A good relationship between the reducibility and high specific surface area and the oxidation performance was found for the synthesized catalysts.

Based on the results mentioned so far, in the present work the effect of varying the molar ratio of citric acid (CA) to metal (La^{3+} + Mn^{2+}) nitrates was investigated in order to improve the physicochemical and catalytic properties of $LaMnO_3$. The prepared samples were characterized by several techniques, such as X-ray diffraction (XRD), specific surface area (N_2 adsorption), inductively coupled plasma atomic emission spectroscopy (ICP-OES), thermogravimetric and differential thermal analysis (TGA/DTA), Fourier Transform Infrared Spectroscopy (FT-IR), temperature-programmed reduction by hydrogen (H_2-TPR), and X-ray photoelectron spectroscopy (XPS). Oxidation tests on the catalytic oxidation of toluene and propene, chosen as target VOCs, were carried out. A Pd/Al_2O_3 catalyst containing 1 wt % Pd was used as the reference for oxidation tests during three cycles. The stability in toluene conversion over the prepared $LaMnO_3$ perovskites was further evaluated through long-term runs (24 h) performed at ~17% of toluene.

2. Results and Discussion

2.1. Characterization

The $LaMnO_3$ samples prepared after calcination at 750 °C were characterized by XRD. Diffraction patterns are shown in Figure 1 for samples prepared with a low molar ratio of CA to total metal ions (La^{3+} + Mn^{2+}) (a), medium molar ratio (b), and high molar ratio (c), respectively. The diffraction lines of the $LaMnO_3$ phase were in good agreement with those of the reference $La_{0.951}Mn_{0.951}O_3$ (PDF 89-8775) with rhombohedral symmetry (space group R-3c), confirming our previous results [27,34]. Moreover, along with the characteristic peaks of the perovskite phase, for molar ratios ranging between 0.5 and 1.5 (see Figure 1a,b), very small features ascribed to the phase Mn_3O_4 (PDF 2-1062) were

detected at 2θ = 38.5°. At a higher concentration of CA, namely values in the range 1.6–2.0, a small peak appeared at 2θ = 29°, attributed to the La_2O_3 phase (PDF 5-602), which was in agreement with the literature [35]. It is worth noting that the XRD patterns of samples from LM1.6 to LM1.8 show both secondary phases, Mn_3O_4 and La_2O_3, while La_2O_3 appeared only in the spectra of LM1.9 and LM2 (see Figure 1c), with the highest amount being detected at a CA to total metal ions (La^{3+} + Mn^{2+}) molar ratio of 2.0. The segregation of a small amount of the Mn_3O_4 phase would suggest the formation of slightly nonstoichiometric perovskite, with the formula $LaMn_{1-x}O_3$, where the electroneutrality of the molecule should be guaranteed by the presence of both Mn^{4+} and Mn^{3+} [16,34]. Conversely, the detection of La_2O_3 should involve the formation of $La_{1-x}MnO_{3-\delta}$ perovskite, where oxygen vacancies formation is likely more favored than Mn^{4+} formation.

Based on the data reported so far, the amount of citric acid used during the $LaMnO_3$ synthesis may affect the phase stoichiometry of the perovskite and Mn oxidation state.

In Table 1 the crystallite sizes of $LaMnO_3$ phase calculated using Scherrer equations are listed, along with the specific surface area values and the chemical composition in terms of Mn and La (wt %), as measured by ICP-OES analysis. The average crystal size varied between 18 and 30 nm, with the smallest sizes at a CA to total metal ions (La^{3+} + Mn^{2+}) molar ratio between 1.1 and 1.5.

The relationship between the surface area and the molar ratio CA to total metal ions (La^{3+} + Mn^{2+}) is displayed in Figure 2. LM1.2 possesses the largest specific surface area equal to 26 $m^2 \times g^{-1}$ and similar values were measured for LM1.1 and LM1.3. For molar ratios between 0.5 and 1.0, the BET values were in the range 9–12 $m^2 \times g^{-1}$. On the other hand, the surface area dramatically decreased from 22 to 5 $m^2 \times g^{-1}$ when increasing the molar ratio from 1.4 to 2.0. It was observed that the higher the concentration of CA, the higher the heat of combustion of the $LaMn(C_6H_5O_7)(NO_3)_3$ intermediate species, which should negatively affect the surface area and crystal size of the resulting LM perovskites [36]. Indeed, when an excess of CA is used, its exothermic decomposition reaction may cause local hot spots inside the powder, determining a decrease in specific surface area of the resulting $LaMnO_3$ samples.

Table 1. Chemical composition and textural properties of $LaMnO_3$ catalysts as a function of citric acid (CA) to metal ions (La^{3+}+ Mn^{3+}) molar ratio.

Samples	Mn [1] (wt %)	La [1] (wt %)	SSA [2] ($m^2 \times g^{-1}$)	d_{XRD} [3] (nm)
LM0.5	22.17	56.20	9	26
LM0.6	20.44	55.66	10	25
LM0.7	22.02	55.74	11	22
LM0.8	21.41	56.20	10	25
LM0.9	21.03	56.49	11	21
LM1	21.58	55.42	12	23
LM1.1	21.25	53.5	25	19
LM1.2	21.75	54.8	26	18
LM1.3	21.42	55.23	25	18
LM1.4	21.50	55.1	22	20
LM1.5	21.55	54.6	21	20
LM1.6	21.56	56.41	13	23
LM1.7	21.22	56.20	12	22
LM1.8	22.06	56.30	5	25
LM1.9	20.77	57	6	28
LM2	20.56	56.72	5	30

[1] La, Mn: mass percentage (wt %) obtained by ICP-OES (inductively coupled plasma atomic emission spectroscopy) analysis; [2] SSA: Specific surface area; [3] d_{XRD}: crystallite size as determined by Scherrer equation.

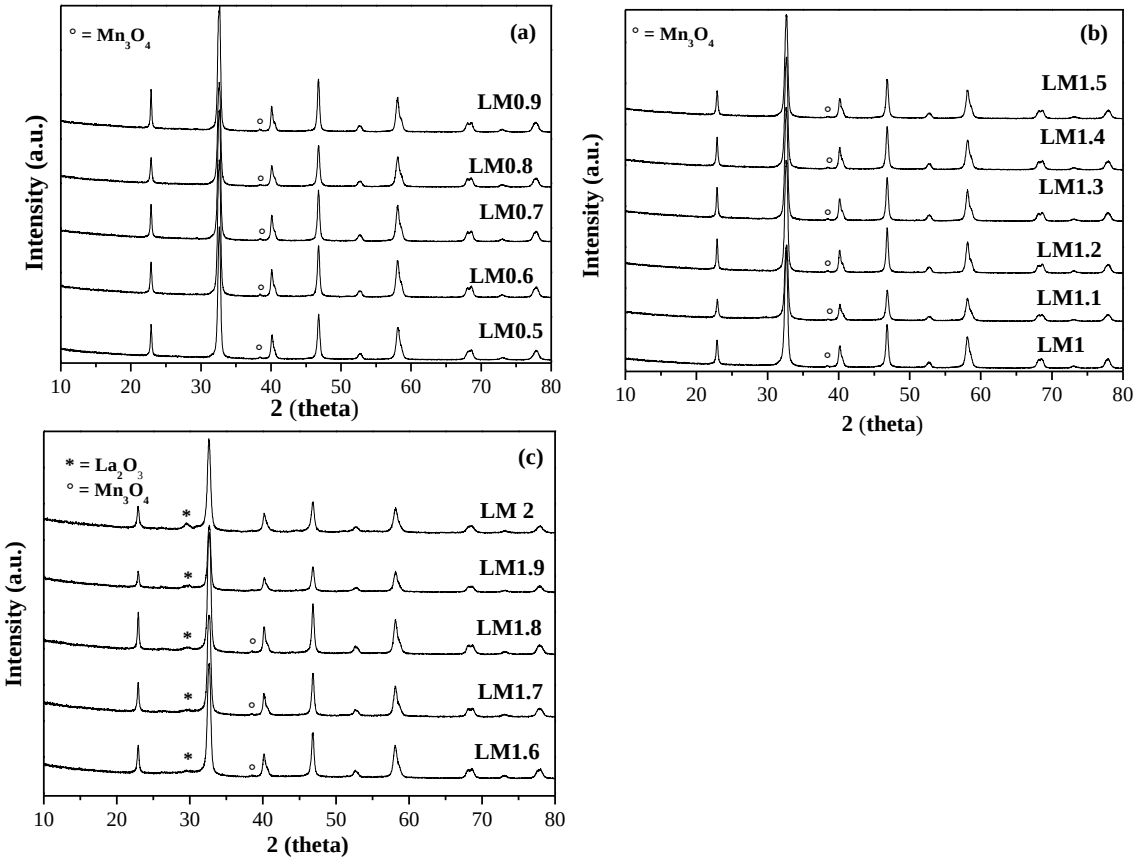

Figure 1. X-ray diffraction (XRD) patterns of $LaMnO_3$ samples prepared with low molar ratio of CA to total metal ions (La^{3+} + Mn^{2+}) (**a**), medium molar ratio (**b**), and high molar ratio (**c**).

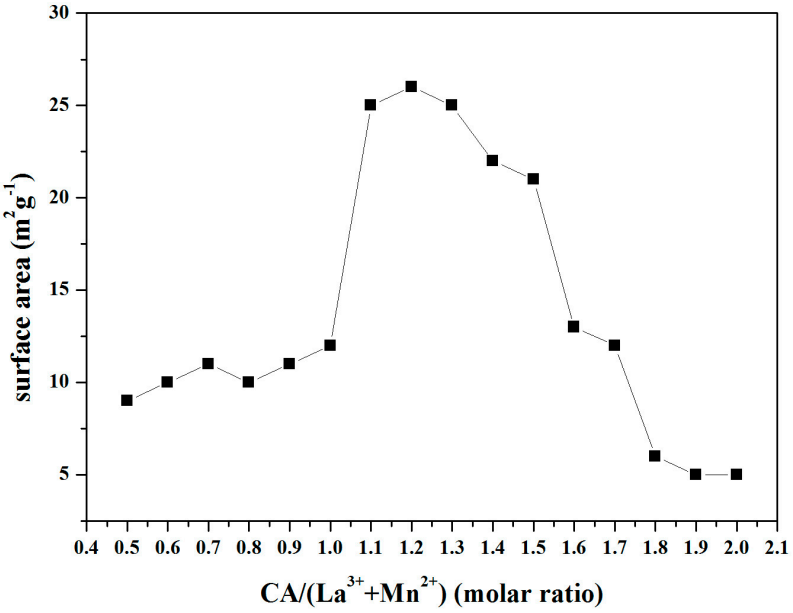

Figure 2. Relationship between the specific surface area of the catalysts and the molar ratio of CA to total metal ions (La^{3+} + Mn^{2+}).

In order to study the thermal stability and crystallization temperature of the catalysts in the form of dried gels, TGA/DTA analyses were carried out under air flow in the temperature range 25–900 °C. The curves registered for selected samples (un-calcined precursor materials) prepared with

low, medium, and high CA to total metal ions (La^{3+} + Mn^{2+}) molar ratio, namely LM0.8 (a), LM1.2 (b), and LM2 (c), are displayed in Figure 3 and compared with those of pure CA (d). For all LM samples, a weight loss ≤10% was observed for runs performed between room temperature and ca. 130–155 °C. No weight loss was detected for pure CA, likely due to the residual adsorbed and hydrated water that may remain in the precursors. This step was followed by two major weight losses (up to ~50–60%) extending between ~200 and 600 °C, corresponding with two exothermic peaks between 250–280 °C and at around 450–470 °C. According to the literature [35] and in line with our previous results [34], in such a temperature range an exothermic reaction between citric acid and nitrates occurs. Moreover, between 400 and 600 °C the decomposition of both carbonate species, such as lanthanum and/or manganese oxycarbonate, as well as the residual nitrate species, may occur, leading to the occurrence of exothermic peaks at ~450 °C. Finally, above 600 °C there was a slight mass decrease, which was ascribed to the formation of the final perovskite phase. The progressive decomposition of the LM gels discussed so far was correlated to the TGA/DTA curves of pure CA, taken as the reference. In such cases, the main weight loss occurred at ~200–280 °C (90%), with an endothermic peak at 220 °C attributed to the decomposition of the citrate into carbonate and oxycarbonate [37]. Total degradation related to the decomposition of carbonate species took place at 280–500 °C (weight loss of 10%).

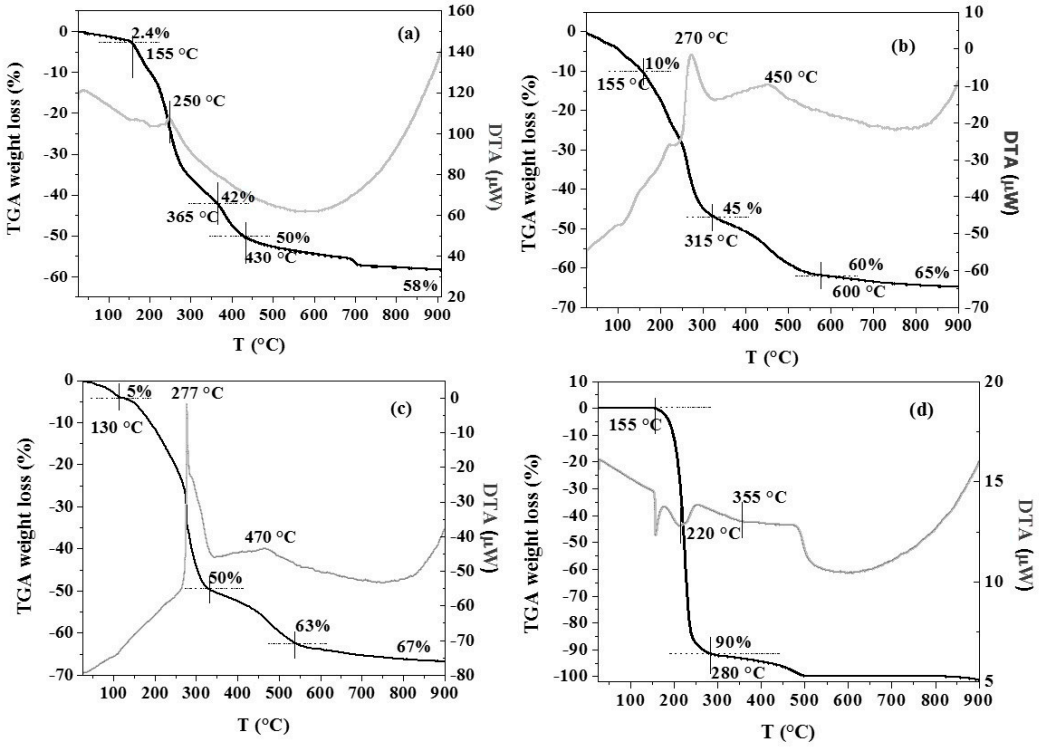

Figure 3. Differential thermal analysis (DTA) and thermogravimetric analysis (TGA) profiles registered under air for selected non-calcined precursor materials (dried gel—catalysts before calcination treatment): (**a**) LM0.8, (**b**) LM1.2, (**c**) LM2, and (**d**) pure CA, used as a reference.

By comparing the TGA curves of the LM samples discussed above, we note that the overall weight loss registered at 900 °C increased as follows: LM0.8 < LM1.2 < LM2, in agreement with the increased amount of CA used in the preparation.

With the purpose of investigating the chemical and structural changes that took place during the combustion process, FT-IR spectra of the dried gels (non-calcined precursor materials) and of the calcined powders were registered in the range from 500 to 4000 cm^{-1}. In Figure 4 the spectra recorded for the sample LM1.2 are shown. The dried gel showed several absorption bands at about 733, 828, 903, 1032, 1280, 1400, 1432, 1595, 1678, 3180, and 3413 cm^{-1} [36,38]. The bands at 3180 and 3413 cm^{-1} are associated with the vibration modes of the O-H groups [38,39]. The bands at 733, 828,

1032, and 1432 cm^{-1} are assigned to the NO_3^- anions [36,40]. The bands at 1400, 1595, and 1678 cm^{-1} are due to the carboxylic groups (COO^-) [36,38,39] and the bands at 903 and 1280 cm^{-1} as well as the abovementioned band at 1032 cm^{-1} could be associated with the C-O stretching mode produced by the drying process of the citric acid foams [39,40]. After calcination, the bands of NO_3^- anions and carboxylic groups disappeared and bands of the O-H reduced significantly in intensity (see Figure 4). The disappearance of such bands in the IR spectra of as-burnt powder suggests that the carboxylic group and NO_3^- ions took part in the reaction during calcination. For the calcined catalyst, a strong band at about 588 cm^{-1} appeared, corresponding to the stretching mode involving the internal motion of a change in length of the Mn-O-Mn or Mn-O bond, as reported in the literature [41]. The last band at 588 cm^{-1} and the small band at 849 cm^{-1} could also be associated with the binding of metal cations, such as La^{3+} with OH groups and oxygen atoms, according to the literature [38,39]. Finally, two bands at 1380 and 1498 cm^{-1} were found after calcination, which are more difficult to assign. Nevertheless, these two bands may be attributed, if compared to those of the dried gel (un-supported precursor materials), to the C-O or M-O stretching modes, which shifted to a low and high wavenumber, respectively. This could indicate that coordination of metal cations by oxygen atoms occurs after the calcination process [39,40].

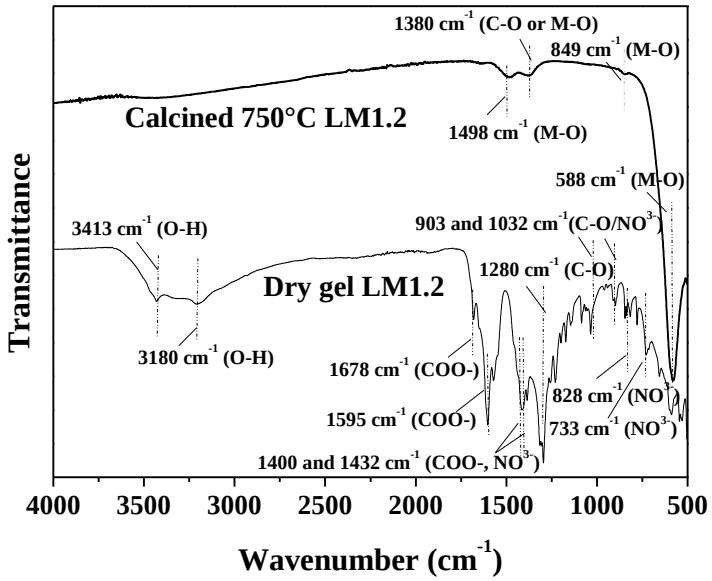

Figure 4. Fourier Transform Infrared Spectroscopy (FT-IR) spectra of the dried gel (non-calcined precursor materials) and calcined powder for LM1.2.

In order to get insights into the relative reducibility of the sample as a function of the CA to total metal ions (La^{3+} + Mn^{2+}) molar ratio, H_2-TPR experiments were carried out over six selected catalysts with low, medium, and high molar ratio values, namely, LM0.8 and LM1, LM1.2 and LM1.3, and LM1.5 and LM1.7. The respective surface area values ranged between 10 and 26 $m^2 \times g^{-1}$. The H_2-TPR profiles are shown in Figure 5, and the corresponding H_2 consumptions and reduction temperatures are summarized in Table 2.

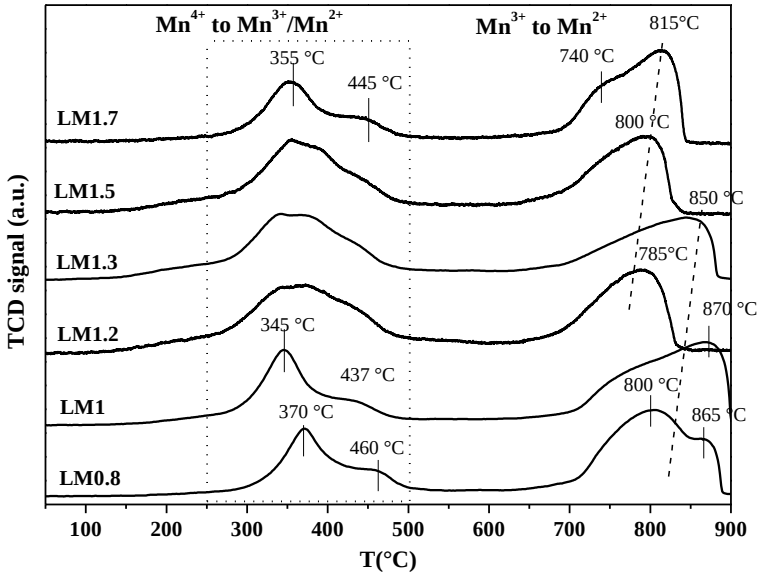

Figure 5. Temperature-programmed reduction by hydrogen (H_2-TPR) profiles of selected $LaMnO_3$ catalysts.

Table 2. Reduction temperature and H_2 uptake of selected $LaMnO_3$ samples.

Samples	H_2-Uptake (mmol × g^{-1})			
	250–500 °C	650–900 °C	Total Uptake	Reducibility % Mn^{n+} to $Mn^{(n-1)+}$ (Calculated Between 250 and 500 °C) [1]
LM0.8	1.073	1.923	2.996	51.9
LM1	1.156	1.883	3.039	55.9
LM1.2	1.296	0.926	2.222	62.7
LM1.3	1.297	1.175	2.472	62.7
LM1.5	1.292	0.922	2.216	62.5
LM1.7	1.066	1.367	2.433	51.6

[1] The reducibility (%) of Mn^{n+} to $Mn^{(n-1)+}$ was calculated on the basis of H_2 consumption in the range 250–500 °C as experimental H_2 uptake (mmol H_2 × g^{-1})/2.067 (mmol H_2 × g^{-1}) × 100.

For all samples, the overall profiles could be divided into two reduction regions: a low-temperature region, at 250–500 °C, and a high-temperature region, above 650 °C. According to the previous results of our group [27,36], the hydrogen consumption below 500 °C was ascribed to the reduction (Mn^{4+} to Mn^{3+}) of some Mn^{4+} present in the perovskite structure. Moreover, based on the hydrogen consumption values, it is likely that the reduction process of Mn^{3+} to Mn^{2+} partially occurred in that temperature range. The shape and temperature of the reduction curves seem to depend on the CA to total metal ions (La^{3+} + Mn^{2+}) molar ratio of the samples and, therefore, on their textural properties. LM0.8, LM1, and LM1.7, characterized by surface area around 10–12 m^2 × g^{-1} and crystal size around 22–25 nm, showed a main peak in the TPR profiles centered between 345 and 370 °C, with a shoulder between 437 and 460 °C. For samples with a larger surface area and relatively smaller crystallites, namely LM1.2, LM1.3, and LM1.5, the reduction peak was broad, suggesting the occurrence of simultaneous reduction processes (Mn^{4+} to Mn^{3+} to Mn^{2+}). As shown in Table 2, the H_2 uptake between 250–500 °C ranged between ~1.0 and 1.3 mmol H_2 × g^{-1}. Such values corresponded to a reduction of ~52–63% of Mn ions contained in 1 g of a sample, with 2.067 mmol H_2 × g^{-1} the stoichiometric amount of hydrogen required for the reduction (Mn^{n+} to $Mn^{(n-1)+}$) of 4.135 mmol of Mn × g^{-1} of perovskite. Samples LM1.2, LM1.3, and LM1.5 showed the highest reducibility below 500 °C; this finding correlates well with the formation of a slightly nonstoichiometric $LaMn_{1-x}O_3$ phase with a relatively high content of Mn^{4+} along with the good performances in toluene and propene oxidation registered for such catalysts (see later in the text).

By increasing the temperature above 650 °C, a broad hydrogen consumption peak ranging between ~0.9 and 1.9 mmol $H_2 \times g^{-1}$ was detected; the shape and position of the maximum were different as a function of the samples, as indicated by the dashed lines plotted in Figure 5. However, no direct relationship between the peak position and the morphological and structure properties of the samples was found. The high-temperature hydrogen consumption was assigned to the reduction (Mn^{3+} into Mn^{2+}) of those Mn species with a stable local environment, likely in the bulk of the perovskite structure.

In order to investigate the surface composition and oxidation state of selected LM samples, XPS analyses were also performed. A typical XPS survey spectrum recorded for sample LM1 is shown in Figure 6. The $La3d_{5/2}$ binding energy for all samples studied is 834.0 eV, typical in La(III) in perovskite materials [42]. The experimental Mn2p XPS spectra for the LM catalysts are displayed in Figure 7, whereas the BE values of O1s for the same catalysts are listed in Table 3. The position shapes and spin-orbit separation of the main peaks are very similar. The BE values of $Mn2p_{3/2}$ were close enough to those obtained for Mn_2O_3 at 641.9 eV. Anyway, the presence of the Mn^{4+} ions could not be excluded because of the proximity of their peak to that of the Mn^{3+} ions (642.2 eV) [37]. To quantify the possible presence of Mn(IV), curve fitting was done according to the procedure developed by Biesinger [43].

Peak sets for MnO_2, Mn_2O_3, and MnOOH were used for the fitting of the $Mn2p_{3/2}$ region. As suggested by Biesinger, six peaks were used to simulate the MnO_2 signal, five peaks for Mn_2O_3, and six peaks for MnO. In Figure 7 experimental and fitted Mn2p XP spectra for selected LM samples are displayed. Mn(III) and Mn (IV) are shown as the sum of the peaks used for the different oxidation states. The fitting procedure indicated the presence of Mn^{3+} as most abundant, and of small amounts (less than 5% for all sample) of Mn^{4+}. No Mn^{2+} was detected. The finding of the same small content of Mn^{4+} detected in all analyzed samples is not contradictory to the formation of a slightly nonstoichiometric $LaMn_{1-x}O_3$ phase, with a relatively high content of Mn^{4+}, as supposed by XRD and in accordance with the TPR results, considering that we are comparing different techniques and XPS is a surface technique.

The constant BE of the $La3d_{5/2}$ and $Mn2p_{3/2}$ levels suggests, according to the results reported in the literature [42], that the chemical bonding for $LaMnO_3$ was not affected by different synthetic procedures. Conversely, there are small differences in the Mn/La atomic ratio as a function of the CA/Mn+La nitrates molar ratio. The Mn surface concentration slightly increased with increasing CA concentration until a maximum was reached for LM1.5 (see Figure 8). The highest surface concentration of Mn detected for samples LM1.2, LM1.3, and LM 1.5 correlates well with their catalytic activity. In particular, LM1.5, showing the highest Mn/La surface atomic ratio, is the most active in toluene and propene oxidation (see later in the text).

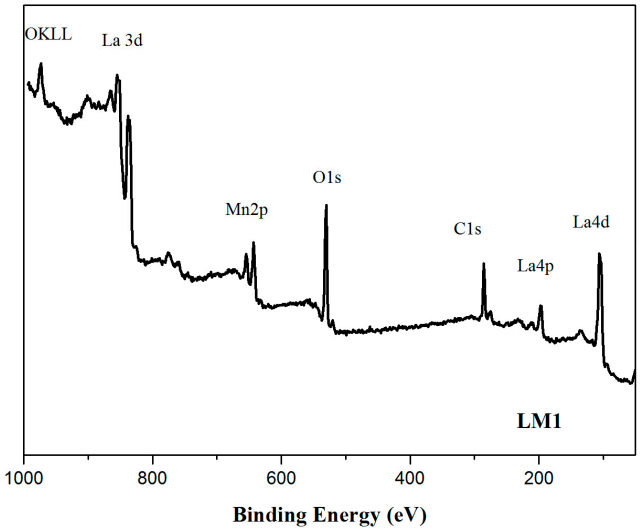

Figure 6. X-ray photoelectron spectroscopy (XPS) survey spectrum recorded for sample LM1.

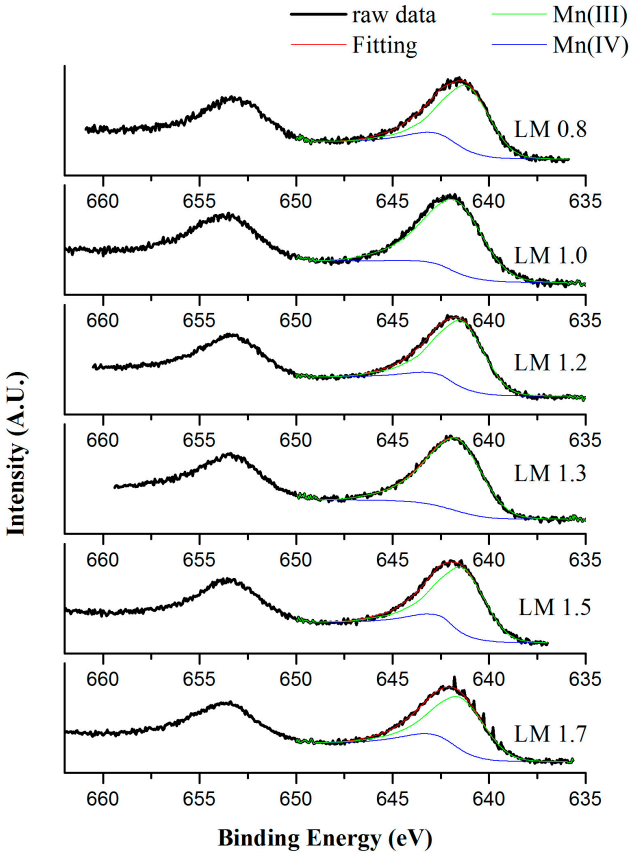

Figure 7. Experimental and fitted Mn2p XP spectra for selected LM samples.

O1s peaks were fitted with two components, a low-energy component at ca. 529.5 eV attributed to oxygen by lattice (O_L) and a high-energy component (531.7 eV) due to hydroxyl oxygen (O_{OH}). The relative percentage of these two components, given in Table 3, can be associated with the formation of $La(OH)_3$ and/or the presence of different oxygen vacancies in the system [44].

Table 3. BE of O1s and Mn2p of selected LM oxides and Mn/La atomic ratio. In parentheses the relative percentage of the two O1s components are given.

Samples	O1s (eV)	Mn/La
LM0.8	529.3 (59%) 531.6 (41%)	0.95
LM1.0	529.6 (70%) 531.9 (30%)	1.00
LM1.2	529.3 (52%) 531.6 (48%)	1.04
LM1.3	529.4 (47%) 531.7 (53%)	1.07
LM1.5	529.5 (66%) 531.7 (34%)	1.27
LM1.7	529.3 (60%) 531.6 (40%)	0.98

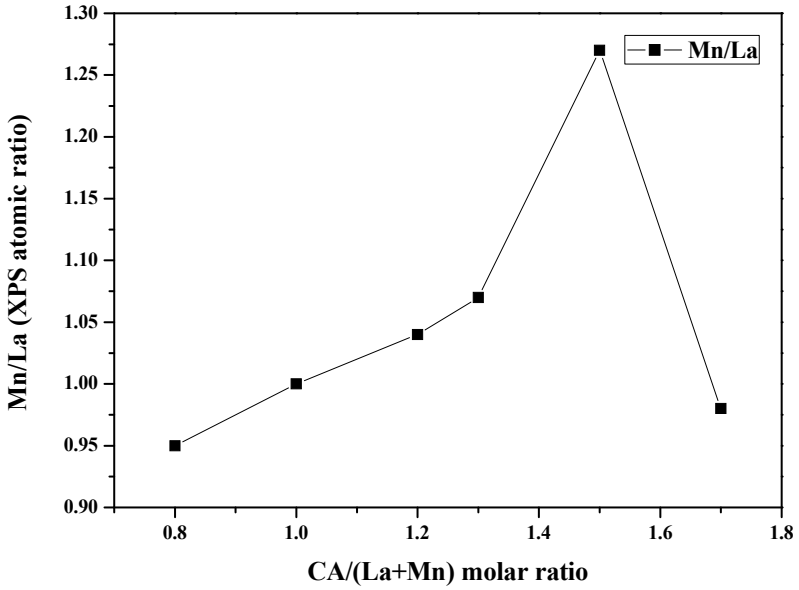

Figure 8. Relationship between the Mn/La surface atomic ratio and the molar ratio of CA to total metal ions (La^{3+} + Mn^{2+}) for selected LM catalysts.

2.2. Toluene and Propene Oxidation Tests

Catalytic activity tests in the toluene and propene oxidation were performed as light-off experiments. The catalyst stability was first evaluated by performing three consecutive catalytic runs for each catalyst. Reproducible results were systematically obtained upon successive toluene and propene oxidation runs. The temperatures corresponding to 10, 50 and 90% of toluene conversion, T10, T50, and T90, respectively, are summarized in Table 4. In Figure 9, the toluene conversion curves achieved for the LM catalysts during the second catalytic run (cooling ramp) are compared to those corresponding to a commercial Pd/Al_2O_3 catalyst containing 1 wt % Pd.

The conversion of toluene increased with the reaction temperature. Thus, a complete conversion of toluene was successfully achieved below 350 °C in all samples. In the entire temperature range, only CO_2 and H_2O were observed when the oxidation of toluene proceeded. Carbon balance was close to 5% in all the catalytic tests. Regarding Figure 9 and Table 4, it can be concluded that the prepared catalysts ranked as follows: LM1.5 ~ LM1.2 ~ LM1.3 > LM1 ~ LM1.7 >> LM0.8. Moreover, the most active ones presented a catalytic performance similar to that of the Pd/Al_2O_3 catalyst used as the reference, especially at T ≥ 250 °C, when conversion values of toluene ≥50% were reached. Pd/Al_2O_3 performed better below 230 °C, giving 10% of toluene conversion at temperatures as low as 214 °C.

Table 4. Catalytic performances of LM catalysts in comparison with Pd (1 wt %)/Al_2O_3 in terms of temperatures for achieving 10, 50 and 90% of toluene conversion. Data were collected upon cooling.

Catalysts	1st Run			2nd Run			3rd Run		
	T_{10} (°C)	T_{50} (°C)	T_{90} (°C)	T_{10} (°C)	T_{50} (°C)	T_{90} (°C)	T_{10} (°C)	T_{50} (°C)	T_{90} (°C)
Pd/Al_2O_3	212	249	276	214	252	279	215	253	281
LM0.8	294	325	345	294	324	346	296	325	351
LM1	245	272	305	251	277	313	255	281	317
LM1.2	233	255	272	237	260	279	243	266	284
LM1.3	238	258	275	243	263	281	247	267	284
LM1.5	233	257	279	237	259	283	239	263	288
LM1.7	251	275	294	255	279	301	260	283	305

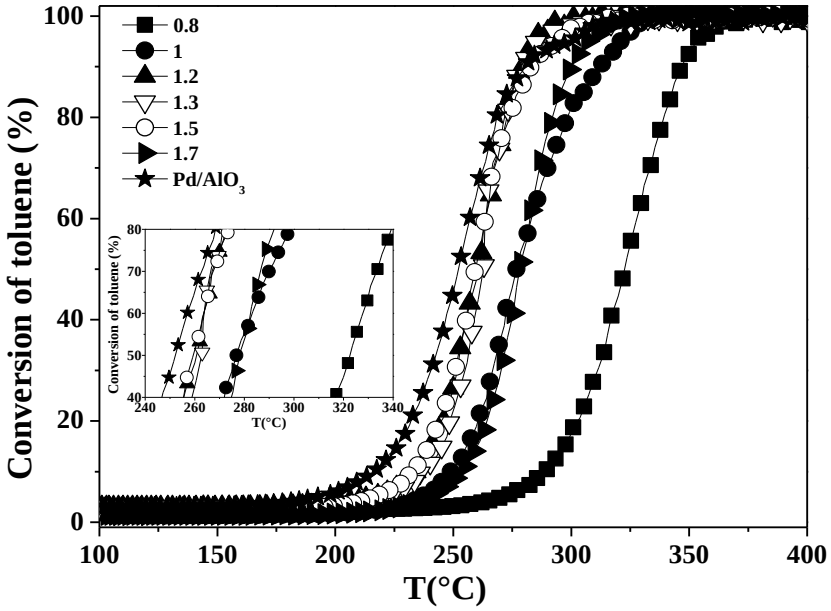

Figure 9. Toluene conversion versus temperature during the second consecutive run (cooling ramp). In the inset, the range of temperature at which conversion values between 40 and 80% were achieved is displayed. The inlet gas composition: 1000 ppm toluene and synthetic air (80/20 vol %) with a total flow of 100 mL × min^{-1} and 100 mg of catalyst.

The reaction rates per gram of catalyst at the same reaction temperature (220 °C) were calculated and are listed in Table 5. These values show the same trend presented in Figure 9, with catalysts LM1.2, LM1.5, and LM1.3 being the most active for toluene total oxidation, whereas LM0.8 presented the worst catalytic performance for the same reaction. These results are in agreement with the high specific surface area of these three catalysts and the lowest SSA of the LM0.8 catalyst. To verify this finding, the reaction rates of perovskite catalysts were calculated per m^2, using the specific surface area calculated by N_2-adsorption analysis (see Table 5). As expected, the same catalytic trend was observed, demonstrating that SSA plays an important role in catalytic activity but is not the only factor that influences the toluene catalytic performance. In addition, the higher activity at the same temperature could also be justified in terms of the oxygen strength (reducibility) of the catalysts, with the three catalysts mentioned (LM1.2, LM1.3, and LM1.5) being the samples that presented the highest reducibility. Therefore, these results allow us to conclude that the catalytic activity in a low-temperature oxidation process depends on the specific surface area, Mn surface concentration, oxidation state, and reducibility.

Table 5. Reaction rate of LM catalysts in terms of gram of catalyst and specific surface area for toluene total oxidation.

Catalysts	Reaction Rate (mol × g^{-1} × s^{-1}) [a]	Reaction Rate (mol × m^{-2} × s^{-1}) [b]
LM0.8	7.00×10^{-5}	7.00×10^{-6}
LM1	3.90×10^{-4}	3.25×10^{-5}
LM1.2	1.70×10^{-3}	6.54×10^{-5}
LM1.3	7.00×10^{-4}	2.80×10^{-5}
LM1.5	9.90×10^{-4}	4.71×10^{-5}
LM1.7	3.10×10^{-4}	2.58×10^{-5}

[a] Reaction rate calculated at 200 °C per gram of catalyst (100 mg for each catalyst); [b] Reaction rate calculated at 200 °C per m^2 (according to the specific surface area obtained using the Brunauer–Emmett–Teller (BET) method; see Table 1).

The catalytic stability of the LM catalysts for the toluene oxidation was further assessed under steady-state conditions at ~17% for 24 h. Figure 10 shows the evolution of the conversion with the time on stream. Conversion values between ~13 and 17% were observed during the entire reaction time. A slight deactivation was observed during the first 4 h of the reaction for all catalysts. After 4 h, LM1.3 exhibited very good stability for the following 20 h (around 16% of toluene conversion); LM0.8 and LM1.2 deactivated up to around 13% of conversion, whereas LM1.5, LM1, and LM1.7 showed intermediate behavior.

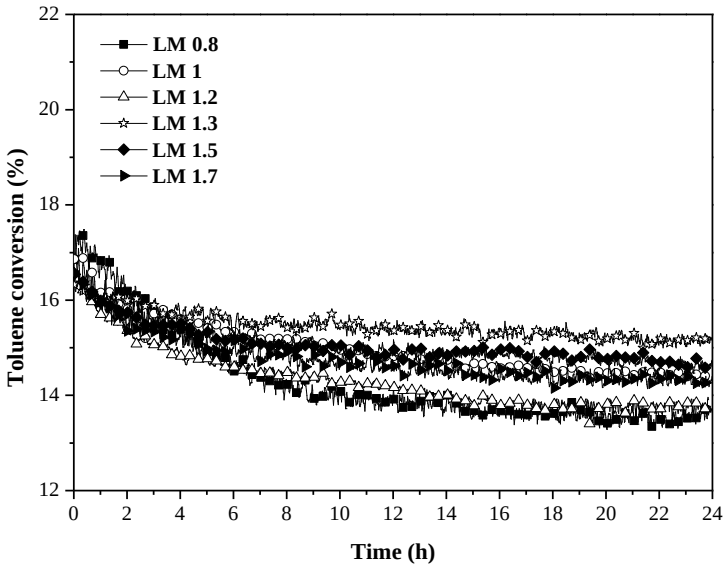

Figure 10. Long-run toluene oxidation test performed at ~17% of toluene conversion during 24 h. The inlet gas composition: 1000 ppm toluene and synthetic air (80/20 vol %) with a total flow of 100 mL × min^{-1} and 100 mg of catalyst.

In order to evaluate the effect of the citric acid concentration on the catalytic performance of LM catalysts, the prepared samples were also tested in the propene oxidation. In Figure 11 propene conversion curves as a function of the temperature (light-off curve) during the second consecutive run (cooling ramp) are displayed. CO_2 and H_2O were the only oxidation products detected during the reaction. The carbon balance was close to 5% in all the catalytic tests.

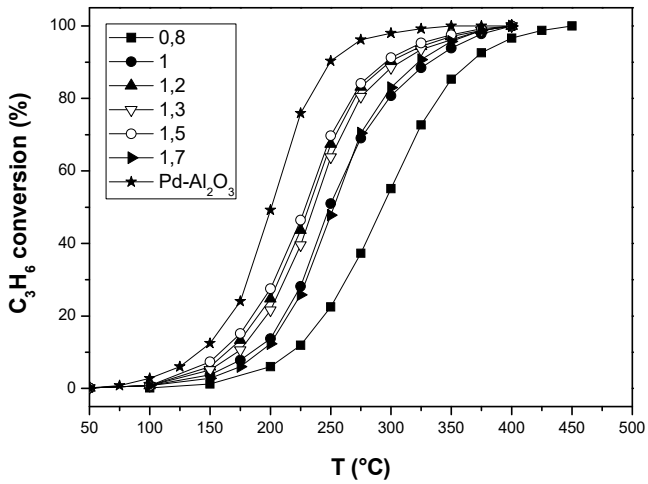

Figure 11. Propene conversion versus temperature during the second consecutive run (cooling ramp). The inlet gas composition: 1000 ppm propene and synthetic air (80/20 vol %) with a total flow of 100 mL × min^{-1} and 100 mg of catalyst.

Table 6 lists the temperatures corresponding to 10, 50 and 90% of propene conversion: T10, T50, and T90, respectively. The rank of activity for LM perovskites was similar to that observed for toluene oxidation, namely LM1.5 ~ LM1.2 ~ LM1.3 > LM1 ~ LM1.7 >> LM0.8, with Pd/Al_2O_3 being the best performing in the entire temperature range.

Table 6. Catalytic performance of LM catalysts in comparison with Pd (1 wt %)/Al_2O_3 in terms of temperatures for achieving 10, 50 and 90% of propene conversion. Data were collected upon cooling.

Catalysts	2nd Run		
	T10 (°C)	T50 (°C)	T90 (°C)
LM0.8	218	293	367
LM1	184	249	333
LM1.2	163	231	299
LM1.3	174	236	309
LM1.5	160	229	298
LM1.7	192	253	324
Pd-Al_2O_3	141	201	250

The reported toluene and propene oxidation data confirm that both processes occur through the same mechanism, likely the Mars-van Krevelen mechanism, involving several redox steps, according to the literature [34,45–47], and pointing to the role of oxidized Mn in activating and oxidizing toluene and propene. Based on that, the higher reducibility and higher surface concentration of Mn oxidized species achieved for LM samples prepared with molar ratio of CA to total metal ions (La^{3+} + Mn^{2+}) ranging between 1.3 and 1.5 is expected to improve the catalytic performance. Moreover, the higher the specific surface area of the catalysts, the higher the number of active oxygen species adsorbed on the surface oxygen vacancies of the samples and easily available for the reaction [47].

3. Materials and Methods

3.1. $LaMnO_3$ Preparation

Citric acid (CA) ($C_6H_8O_7$, Alfa Aesar, Haverhill, MA, USA, 99.5%) and nitrates ($La(NO_3)_3 \times 6H_2O$, Fluka, Seelze, Germany, 99% and $Mn(NO_3)_2 \times 4H_2O$, Alfa Aesar, Haverhill, MA, USA, 98%) were used as metal precursors to prepare the $LaMnO_3$ perovskite-type oxides. Equimolar amounts of the nitrates were mixed and dissolved in distilled water. An amount of CA, corresponding to a CA/Mn+La nitrates molar ratio set from 0.5 to 2, was added at room temperature to the dissolved nitrates. The solution was heated to 80 °C under magnetic stirring for the evaporation of excess water, then dried at 120 °C overnight. Subsequently, the solid was calcined from 25 °C up to 750 °C (5 °C × min^{-1}) for 2 h under air flow. The $LaMnO_3$ catalysts obtained were labeled as LM_x, where x corresponds to the CA/Mn + La nitrates molar ratio and ranges between 0.5 and 2.0. Typically, the catalysts were pressed and sieved after calcination treatment.

3.2. Characterizations

Powder X-ray diffraction (XRD) patterns were recorded on a Bruker D8 X-ray diffractometer (Billerica, MA, USA) at room temperature with CuKα radiation (λ = 1.5418 Å). The diffractograms were recorded for 2θ values between 10 and 80° using a 0.02° step with an integration time of 4 s. The diffraction patterns have been indexed by comparison with the Joint Committee on Powder Diffraction Standards (JCPDS) files.

Nitrogen adsorption isotherms at −196 °C were obtained using a Micromeritics Tristar 3000 instrument (Ottawa, Canada). Before measurement, the samples were outgassed at 300 °C for 3 h. The specific surface area (SSA) of each sample was obtained using the Brunauer–Emmett–Teller (BET) method.

Inductively-Coupled Plasma Optical Emission Spectroscopy (HORIBA Jobin Yvon Activa ICP-OES, Kyoto, Japan) was used for elementary analysis. The powder samples were dissolved in acidic media (a mixture of HF, H_2SO_4, and HNO_3 solutions) and the analyses were performed on the prepared solutions using calibration standards.

Thermogravimetric and differential thermal analyses (TGA/DTA) were carried out over the dried catalysts (non-calcined catalysts) in the temperature range 25–900 °C (10 °C × min^{-1}) on a SETARAM Setsys Evolution 12 calorimeter (Caluire, France), using 2–7 mg of sample, under flowing air.

The Fourier Transform Infrared (FT-IR) transmission spectra were recorded between 400 and 4000 cm^{-1} with a Spectrum Two FT-IR Spectrometer PerkinElmer (Waltham, MA, USA), using self-supporting KBr disks. Before recording FT-IR spectra, the samples were pretreated in an oven overnight at 100 °C.

Temperature-programmed reduction (TPR) runs were performed in a commercial BELCAT-B (Bel Japan, Inc., Toyonaka, Japan) unit with TCD detection. Samples (ca. 0.1 g), were loaded into a U-shaped quartz tube and pre-treated at 250 °C for 30 min under Ar flow (50 cm^3 × min^{-1}). After cooling down, the temperature was ramped from room temperature to 900 °C (10 °C × min^{-1}), using a reducing gas mixture consisting of 5 vol % H_2 in Ar (50 cm^3 × min^{-1}).

The X-ray photoelectron spectroscopy (XPS) analyses of the powders were performed with a VG Microtech ESCA 3000 Multilab (VG Scientific, Sussex, UK), using Al Kα source (1486.6 eV) run at 14 kV and 15 mA, and CAE analyzer mode. For the individual peak energy regions, a pass energy of 20 eV set across the hemispheres was used. The constant charging of the samples was subtracted by referencing all the energies to the C 1s, peak energy set at 285.1 eV, arising from adventitious carbon. Analysis of the peaks was performed using the CASA XPS software (http://www.casaxps.com/berlin/). The binding energy values are quoted with a precision of ±0.15 eV and the atomic percentage with a precision of ±10%.

3.3. Catalytic Tests

Catalytic tests of toluene and propene were carried out using 100 mg of catalyst (with grain diameters between 50 and 100 μm) mixed with silicon carbide (mass ratio 1:1) to avoid any hot spots. The catalyst was immobilized over a quartz wool plug in a U-shaped reactor and the reactive mixture, containing 1000 ppm C_3H_6 or 1000 ppm C_7H_8 and synthetic air (80/20 vol %) with a total flow of 100 mL × min^{-1} and a GHSV of 60,000 mL × h^{-1} × g^{-1}, was then flowed over it. The concentration of reactants was adjusted by using, for toluene, a saturator coupled with Corto CD20F cryothermostat (Julabo, Seelbach, Germany) and by mass flow controllers (BROOKS) for other gases. Each catalytic run was performed as follows: introduction of the reaction mixture at room temperature, heating at a ramp rate of 5 °C × min^{-1} up to 100 °C for 30 min, in order to stabilize the system. Subsequently, a second temperature ramp of 2 °C × min^{-1} was applied up to 400 °C. After such treatment, all catalysts were tested upon cooling the reactor down to room temperature. This sequence was repeated three times. The temperature was measured and controlled by an oven surrounding the reactor with a thermocouple located inside the catalytic bed.

In order to compare the activity of our catalysts with a commercial reference, a catalyst with composition Pd (1 wt %)/Al_2O_3 was used in the toluene oxidation for three cycles.

Long-term toluene oxidation tests running for 24 h at ~17% toluene conversion were also performed in order to evaluate the catalytic stability. The same reactive mixture, containing 1000 ppm C_7H_8 and synthetic air (80/20 vol %) with a total flow of 100 mL × min^{-1}, was used for long-term experiments. In this case, the catalytic performance of catalysts was measured as follows: the reactive mixture was flowed over the catalyst at room temperature before heating at a ramp rate of 5 °C × min^{-1} up to 100 °C for 30 min. Subsequently, a second temperature ramp of 2 °C × min^{-1} was applied up to 400 °C. After that, the catalysts were tested upon cooling the reactor down until the temperature achieved ~17% toluene conversion, staying at this temperature for 24 h.

Toluene, propene, and other possible partially oxidized products were analyzed using a micro gas chromatograph (R3000, SRA, Marcy l'Etoile, France). For CO and CO_2 online infrared-ultraviolet analyzers (ROSEMOUNT Xstream, Emerson Electric, St. Louis, MO, USA) were used. No other organic hydrocarbons were detected among the reaction products. Carbon balance was close to 5% in all the catalytic tests.

4. Conclusions

In this work, the effect of the preparation method, citrate sol–gel method, and molar ratio of citric acid (CA) to metal (La^{3+} + Mn^{2+}) nitrates on the physicochemical properties and the catalytic performance of $LaMnO_3$ perovskites was demonstrated. The amount of citric acid used during the $LaMnO_3$ synthesis affects the specific surface area, crystalline phase of the perovskite, and Mn species reducibility. For molar ratios ranging between 0.5 and 1.5, the segregation of a small amount of Mn_3O_4, detected by XRD, suggested the formation of a slightly nonstoichiometric $LaMn_{1-x}O_3$ phase with a relatively high content of Mn^{4+} and high reducibility.

In the oxidation of toluene, the catalysts LM1.2, LM1.3, and LM1.5 showed the best performance in the temperature range 150–400 °C and compared favorably with Pd over alumina, taken as a reference. LM0.8 performed poorly, while LM1 and LM1.7 exhibited intermediate behavior. A similar trend in propene conversion in the temperature range 100–400 °C was registered for the same set of catalysts. Under steady-state conditions at ~17% of toluene conversion for 24 h, LM1.3 exhibited the best activity and durability (stable values of toluene conversion, around 16%, were registered).

In conclusion, the three best-performing $LaMnO_3$ catalysts are those forming a slightly nonstoichiometric $LaMn_{1-x}O_3$ phase. They are characterized by the highest specific surface area, the highest Mn surface concentration, and Mn reducibility. All these factors play a fundamental role in toluene and propene oxidation reactions.

Author Contributions: This study was conducted through contributions of all authors. S.G., L.F.L. and A.G.-F. have coordinated the work and have written the manuscript. Z.S. and F.P. have prepared the samples, performed morphological and structural characterizations and toluene oxidation tests. G.P. has made TPR experiments and propene oxidation tests. V.L.P. performed XPS analyses. J.L.V. collaborated to the exploitation of data and writing the manuscript.

Funding: This research received no external funding.

Acknowledgments: This work was financially supported by the Libyan Ministry, Université Lyon 1 and CNRS (PICs program PROXIVOC 2015–2017). The contribution of the joint Ph.D. Program between the Libyan Scholarship Council, the Institute de Recherches sur la Catalyse et l'Environnement de Lyon (IRCELYON), University Claude Bernard Lyon 1 (UCBL1), the Istituto per lo Studio dei Materiali Nanostrutturati (ISMN) of Palermo and the University of Castilla La Mancha, Spain is also acknowledged.

Conflicts of Interest: The authors declare no conflict of interest.

References

1. Holtappels, P.; Bagger, C. Fabrication and performance of advanced multi-layer SOFC cathodes. *J. Eur. Ceram. Soc.* **2002**, *22*, 41–48. [CrossRef]
2. Yuasa, M.; Shimanoe, K.; Teraoka, Y.; Yamazoe, N. Preparation of carbon-supported nano-sized $LaMnO_3$ using reverse micelle method for energy-saving oxygen reduction cathode. *Catal. Today* **2007**, *126*, 313–319. [CrossRef]
3. Zhu, C.; Nobuta, A.; Nakatsugawa, I.; Akiyama, T. Solution combustion synthesis of $LaMO_3$ (M = Fe, Co, Mn) perovskite nanoparticles and the measurement of their electrocatalytic properties for air cathode. *Int. J. Hydrogen Energy* **2013**, *38*, 13238–13248. [CrossRef]
4. Nagaev, E.L. Colossal-magnetoresistance materials: Manganites and conventional ferromagnetic semiconductors. *Phys. Rep.* **2001**, *346*, 387–531. [CrossRef]
5. Wu, X.; Xu, L.; Weng, D. The NO selective reduction on the $La_{1-x}Sr_xMnO_3$ catalysts. *Catal. Today* **2004**, *90*, 199–206. [CrossRef]

6. Giannakis, A.E.; Ladavos, A.K.; Pomonis, P.J. Preparation, characterization and investigation of catalytic activity for NO+CO reaction of $LaMnO_3$ and $LaFeO_3$ perovskites prepared via microemulsion method. *Appl. Catal. B Environ.* **2004**, *49*, 147–158. [CrossRef]
7. Kim, C.H.; Qi, G.; Dahlberg, K.; Li, W. Strontium-Doped Perovskites Rival Platinum Catalysts for Treating NO_x in Simulated Diesel Exhaust. *Nature* **2010**, *327*, 1624–1627.
8. Ciambelli, P.; Palma, V.; Tikhov, S.F.; Sadykov, V.A.; Isupova, L.A.; Lisi, L. Catalytic activity of powder and monolith perovskites in methane combustion. *Catal. Today* **1999**, *47*, 199–207. [CrossRef]
9. Song, K.S.; Xing, H.; Sang, C.; Kim, D.; Kang, S.K. Catalytic combustion of CH_4 and CO on $La_{1-x}M_xMnO_3$ perovskites. *Catal. Today* **1999**, *47*, 155–160. [CrossRef]
10. Cimino, S.; Pirone, R.; Lisi, L. Zirconia supported $LaMnO_3$ monoliths for the catalytic combustion of methane. *Appl. Catal. B Environ.* **2002**, *35*, 243–254. [CrossRef]
11. Gallagher, P.K.; Johnson, D.W.; Remeika, J.P.; Schrey, F.; Trimble, L.E.; Vogel, E.M.; Voorhoeve, R.J.H. The activity of $La_{0.7}Sr_{0.3}MnO_3$ without Pt and $La_{0.7}Pb_{0\cdot3}MnO_3$ with varying Pt contents for the catalytic oxidation of CO. *Mater. Res. Bull.* **1975**, *10*, 529–538. [CrossRef]
12. Gallagher, P.K.; Johnson, D.W.; Vogel, E.M.; Schrey, F. Effects of the Pt content of $La_{0.7}Pb_{0.3}MnO_3$ on its catalytic activity for the oxidation of CO in the presence of SO_2. *Mater. Res. Bull.* **1975**, *10*, 623–628. [CrossRef]
13. Song, K.S.; Kang, S.K.; Kim, S.D. Preparation and characterization of Ag/MnO_x/perovskite catalysts for CO oxidation. *Cat. Lett.* **1997**, *49*, 65–68. [CrossRef]
14. Li, W.B.; Wang, J.X.; Gong, H. Catalytic combustion of VOCs on non-noble metal catalysts. *Catal. Today* **2009**, *148*, 81–87. [CrossRef]
15. Stege, W.P.; Cadús, L.E.; Barbero, B.P. $La_{1-x}Ca_xMnO_3$ perovskites as catalysts for total oxidation of volatile organic compounds. *Catal. Today* **2011**, *172*, 53–57. [CrossRef]
16. Zhang, C.; Wang, C.; Zhan, W.; Guo, Y.; Lu, G.; Baylet, A.; Giroir-Fendler, A. Catalytic oxidation of vinyl chloride emission over $LaMnO_3$ and $LaB_{0.2}Mn_{0.8}O_3$ (B = Co, Ni, Fe) catalysts. *Appl. Catal. B Environ.* **2013**, *129*, 509–516. [CrossRef]
17. Gallagher, P.K.; Johnson, D.W.; Vogel, E.M.; Schrey, F. Studies of some supported perovskite oxidation catalysts. *Mater. Res. Bull.* **1974**, *9*, 1345–1352. [CrossRef]
18. Yamazoe, N.; Teraoka, Y. Oxidation catalysis of perovskites—Relationships to bulk structure and composition (valency, defect, etc.). *Catal. Today* **1990**, *8*, 175–199. [CrossRef]
19. Spinicci, R.; Faticanti, M.; Marini, P.; De Rossi, S.; Porta, P. Catalytic activity of $LaMnO_3$ and $LaCoO_3$ perovskites towards VOCs combustion. *J. Mol. Catal. A Chem.* **2003**, *197*, 147–155. [CrossRef]
20. Ivanov, D.V.; Sadovskaya, E.M.; Pinaeva, L.G.; Isupova, L.A. Influence of oxygen mobility on catalytic activity of La-Sr-Mn-O composites in the reaction of high temperature N_2O decomposition. *J. Catal.* **2009**, *267*, 5–13. [CrossRef]
21. Bell, R.J.; Millar, G.J.; Drennan, J. Influence of synthesis route on the catalytic properties of $La_{1-x}Sr_xMnO_3$. *Solid State Ion.* **2000**, *131*, 211–220. [CrossRef]
22. Royer, S.; Bérubé, F.; Kaliaguine, S. Effect of the synthesis conditions on the redox and catalytic properties in oxidation reactions of $LaCo_{1-x}Fe_xO_3$. *Appl. Catal. A Gen.* **2005**, *282*, 273–284. [CrossRef]
23. Wachowski, L. Influence of the method of preparation on the porous structure of perovskite oxides. *Surf. Coat. Technol.* **1986**, *29*, 303–311. [CrossRef]
24. Baythoun, M.S.G.; Sale, F.R.J. Production of strontium-substituted lanthanum manganite perovskite powder by the amorphous citrate process. *Mater. Sci.* **1982**, *17*, 2757–2769. [CrossRef]
25. Taguchi, H.; Yamada, S.; Nagao, M.; Ichikawa, Y.; Tabata, K. Surface characterization of $LaCoO_3$ synthesized using citric acid. *Mater. Res. Bull.* **2002**, *37*, 69–76. [CrossRef]
26. Ng Lee, Y.; Lago, R.M.; Fierro, J.L.G.; Gonzalez, J. Hydrogen peroxide decomposition over $Ln_{1-x}A_xMnO_3$ (Ln = La or Nd and A = K or Sr) perovskites. *Appl. Catal. A Gen.* **2001**, *215*, 245–256.
27. Zhang, C.; Guo, Y.; Boreave, A.; Retailleau, L.; Baylet, A.; Giroir-Fendler, A. $LaMnO_3$ perovskite oxides prepared by different methods for catalytic oxidation of toluene. *Appl. Catal. B Environ.* **2014**, *490*, 148–149. [CrossRef]
28. Tejuca, L.G.; Fierro, J.L.G.; Tascon, J.M.D. Structure and Reactivity of Perovskite-Type Oxides. *Adv. Catal.* **1989**, *36*, 237–328.
29. Wachowski, L.; Zielinski, S.; Burewicz, A. Preparation, stability and oxygen stoichiometry in perovskite-type binary oxides. *Acta Chim. Acad. Sci. Hung.* **1981**, *106*, 217–225.

30. Kaliaguine, S.; Van Neste, A. Process for Synthesizing Perovskites Using High Energy Milling. U.S. Patent 6017504, 25 January 2000.
31. Kaliaguine, S.; Van Neste, A. Process for Synthesizing Metal Oxides and Metal Oxides Having a Perovskite or Perovskite-Like Crystal Structure. U.S. Patent 6770256, 3 August 2004.
32. Mali, A.; Ataie, A. Structural characterization of nano-crystalline $BaFe_{12}O_{19}$ powders synthesized by sol–gel oxidation route. *Scr. Mater.* **2005**, *53*, 1065–1070. [CrossRef]
33. Yue, Z.X.; Guo, W.Y.; Zhou, J.; Gui, Z.J.; Li, L.T. Synthesis of nanocrystilline ferrites by sol–gel combustion process: The influence of pH value of solution. *J. Magn. Magn. Mater.* **2004**, *270*, 216–223. [CrossRef]
34. Sihaib, Z.; Puleo, F.; Garcia-Vargas, J.M.; Retailleau, L.; Descorme, C.; Liotta, L.F.; Valverde, J.L.; Gil, S.; Giroir-Fendler, A. Manganese oxide-based catalysts for toluene oxidation. *Appl. Catal. B Environ.* **2017**, *209*, 689–700. [CrossRef]
35. Ghiasi, E.; Malekzadeh, A.; Ghiasi, M. Moderate concentration of citric acid for the formation of $LaMnO_3$ and $LaCoO_3$ nano-perovskites. *J. Rare Earths* **2013**, *31*, 997–1002. [CrossRef]
36. Taguchi, H.; Matsuura, S.I.; Nagao, M.; Choso, T.; Tabata, K. Synthesis of $LaMnO_{3+\delta}$ by Firing Gels Using Citric Acid. *J. Solid State Chem.* **1997**, *129*, 60–65. [CrossRef]
37. Hammami, R.; Aïssa, S.B.; Batis, H. Effects of thermal treatment on physicochemical and catalytic properties of lanthanum manganite $LaMnO_{3+y}$. *Appl. Catal. A Gen.* **2009**, *353*, 145–153. [CrossRef]
38. Predoana, L.; Malic, B.; Kosec, M.; Carata, M.; Caldararu, M.; Zaharescu, M. Characterization of $LaCoO_3$ powders obtained by water-based sol–gel method with citric acid. *J. Eur. Ceram. Soc.* **2007**, *27*, 4407–4411. [CrossRef]
39. Gómez-Cuaspud, J.A.; Valencia-Ríos, J.S.; Carda-Castelló, J.B. Preparation and characterization of perovskite oxides by polymerization-combustion. *J. Chil. Chem. Soc.* **2010**, *55*, 445–449. [CrossRef]
40. Berger, D.; Matei, C.; Papa, F.; Macovei, D.; Fruth, V.; Deloume, J.P. Pure and doped lanthanum manganites obtained by combustion method. *J. Eur. Ceram. Soc.* **2007**, *27*, 4395–4398. [CrossRef]
41. Nagabhushana, B.M.; Chakradhar, R.P.S.; Ramesh, K.P.; Shivakumara, C.; Chandrappa, G.T. Combustion synthesis, characterization and metal–insulator transition studies of nanocrystalline $La_{1-x}Ca_xMnO_3$ ($0.0 \leq x \leq 0.5$). *Mater. Chem. Phys.* **2007**, *102*, 47–52. [CrossRef]
42. Taguchi, H.; Sugita, A.; Nagao, M.; Tabata, K. Surface characterization of $LaMnO_{3+\delta}$ powder annealed in air. *J. Solid State Chem.* **1995**, *119*, 164–168. [CrossRef]
43. Biesinger, M.C.; Payne, B.P.; Grosvenor, A.P.; Lau, L.W.M.; Gerson, A.R.; Smart, R.S.C. Resolving surface chemical states in XPS analysis of first row transition metals, oxides and hydroxides: Cr, Mn, Fe, Co and Ni. *Appl. Surf. Sci.* **2011**, *257*, 2717–2730. [CrossRef]
44. Kuyyalil, J.; Newby, D., Jr.; Laverock, J.; Yu, Y.; Cetin, D.; Basuc, S.N.; Ludwig, K.; Smith, K.E. Vacancy assisted SrO formation on $La_{0.8}Sr_{0.2}Co_{0.2}Fe_{0.8}O_{3-\delta}$ surfaces—A synchrotron photoemission study. *Surf. Sci.* **2015**, *642*, 33–38. [CrossRef]
45. Liu, P.; He, H.; Wei, G.; Liu, D.; Liang, X.; Chen, T.; Zhu, J.; Zhu, R. An efficient catalyst of manganese supported on diatomite for toluene oxidation: Manganese species, catalytic performance, and structure-activity relationship. *Microporous Mesoporous Mater.* **2017**, *239*, 101–110. [CrossRef]
46. Doornkamp, C.; Ponec, V. The universal character of the Mars and Van Krevelen mechanism. *J. Mol. Catal. A Chem.* **2000**, *162*, 19–32. [CrossRef]
47. Liotta, L.F.; Ousmane, M.; Di Carlo, G.; Pantaleo, G.; Deganello, G.; Marcì, G.; Retailleau, L.; Giroir-Fendler, A. Total oxidation of propene at low temperature over Co_3O_4–CeO_2 mixed oxides: Role of surface oxygen vacancies and bulk oxygen mobility in the catalytic activity. *Appl. Catal. A Gen.* **2008**, *347*, 81–88. [CrossRef]